Detection of planetary terrain features

Suraphol Udomkesmalee and Luisa De Antonio

Jet Propulsion Laboratory, California Institute of Technology
Pasadena, California 91109

ABSTRACT

A particular aspect of autonomous target tracking for planetary bodies, detection of "distinct" features appearing in the scene, is addressed. Using the gray level cooccurrence (GLC) matrices, object detection is done by applying measures (metrics) defined on GLC matrices to different regions on the image plane. The decision logic for detecting "unique" features can then be implemented using a supervised or unsupervised parametric method on a set of GLC-metric measurements. Detailed algorithms and test results based on Voyager image data are presented.

Keywords: feature detection, planetary terrains, detection metrics, cooccurrence matrices, texture discrimination

1. INTRODUCTION

Onboard feature detection capability for planetary spacecraft can prevent the loss of opportunities to conduct detailed investigations of serendipitous targets such as erupting volcanoes on Jupiter's moon Io, the moon of Asteroid Ida, geysers on Neptune's moon Triton, and other such features. We have just begun the research to detect, track, and point to targets of interest that consist of celestial bodies terrain features.[1-3] The geometric and radio metric simplicity of planetary features compared to the more complicated terrestrial scenes addressed by the general computer vision discipline should permit us to quickly advance and mature this intelligent, vision-based technology for space exploration. Although the target features and background definitions are somewhat nebulous, some predictable features, such as circular spots, craters, mountains, valleys, and line markings are characteristic of surveyed planets and satellites in our solar system (see Fig. 1).

In this paper, we will address a particular aspect of autonomous target tracking for planetary bodies, detection of "distinct" objects appearing in the scene. General functional requirements for planetary exploration based on image processing and pattern recognition have been addressed[1]. Note that we will use the term "feature" to denote the distinct object that can be used to map the targeted celestial body and to initiate/plan detailed investigations through spacecraft maneuvers and pointing to meet desired science objectives.

Although high resolution and multispectral images are available in planetary exploration, object detection based on step-wise analysis of spectral, spatial, and texture properties is not practical in this case. Besides the flight-computer-processing throughput and memory limitations, the use of the science imaging instruments (multispectral images are science-driven and achieved through color filters) may not be appropriate (because of the camera characteristics--very narrow field-of-view, sharply focussed, etc.) for designating feature points for science observations. Furthermore, the required a priori knowledge concerning the multidimensional characteristics of desired features will be extremely difficult to come by. Our current thinking favors a lower resolution, wider field-of-view, and fast-readout camera for detecting and designating science pointing operations.

The use of the gray level cooccurrence (GLC) matrices[5] proved effective in characterizing distributed and textured patterns.[6] Object detection is done by applying measures (metrics) defined on GLC matrices to different regions on the image plane. The decision logic for detecting "unique" objects can then be implemened using a supervised *or* unsupervised parametric method for a set of GLC-metric measurements (this is basically a systematic approach for thresholding). To evaluate the effectiveness of this texture-based image analysis on planetary terrains, the conventional texture measures[7] were employed. Detailed analysis in detecting planetary features was conducted using real images from Voyager image data. Preliminary results are quite promising. Efficient detection of distinct planetary features may be achieved using only a single GLC-based matric.

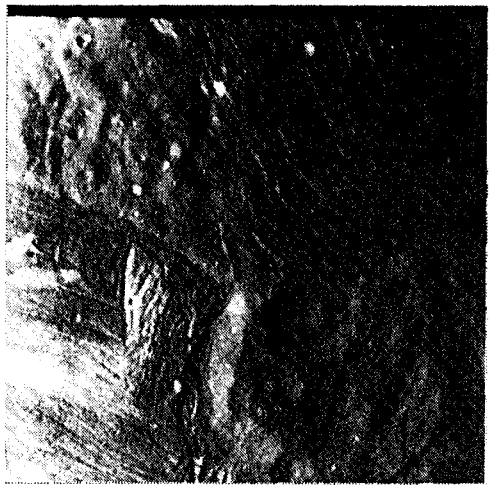

(a) Uranus' moon Miranda

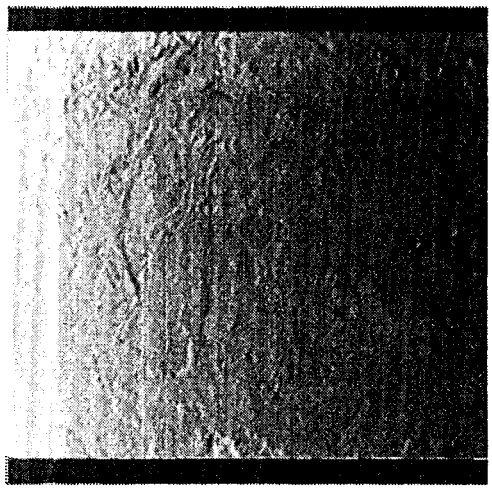

(b) Neptune's moon Triton

(c) Jupiter's moon 10

(d) Jupiter

Fig. 1. Typical planetary features from the Voyager archive. These images are 800x800 pixels. Regions from these images are selected for evaluating the performance of GLC-based feature detection metrics.

2. CANDIDATE DETECTION METRICS

A GLC matrix S(6,7) = [$s(i, j, \delta, 7)$] estimates the second-order probability of having a transition from gray level i to gray level j for any two pixels within the tile 7 that are separated by δ. δ can be defined either in the polar form (d, θ) or in Cartesian (Ax, Ay). Thus, GLC matrices are L×L, where L is the number of gray levels. Candidate GLC-based metrics[7] are inertia, cluster shade, cluster prominence, local homogeneity, energy, and entropy:

Inertia

$$I(6, \quad T) \quad = \sum_{i=0}^{1,-1} \sum_{j=0}^{L-1} (i - j)^2 \, s(i, j, \delta, T)$$

Cluster shade

$$A(\delta, T) = \sum_{i=0}^{L-1} \sum_{j=0}^{L-1} (i + j - \mu_x - \mu_y)^3 s(i, j, \delta, T)$$

Cluster prominence

$$B(\delta, T) = \sum_{i=0}^{L-1} \sum_{j=0}^{L-1} (i + j - \mu_x - \mu_y)^4 s(i, j, \delta, T)$$

Local homogeneity

$$L(\delta, T) = \sum_{i=0}^{L-1} \sum_{j=0}^{L-1} \frac{1}{1 + (i - j)^2} s(i, j, \delta, T)$$

Energy

$$E(\delta, T) = \sum_{i=0}^{L-1} \sum_{j=0}^{L-1} [s(i, j, \delta, T)]^2$$

Entropy

$$H(\delta, T) = \sum_{i=0}^{L-1} \sum_{j=0}^{L-1} s(i, j, \delta, T) \log(s(i, j, \delta, T))$$

where $\mu_x = \sum_{i=0}^{L-1} i \sum_{j=0}^{L-1} s(i, j, \delta, T)$ and $\mu_y = \sum_{i=0}^{L-1} \sum_{j=0}^{L-1} j\, s(i, j, \delta, T)$.

Intuitively, inertia highlights random texture; cluster shade and cluster prominence exphasize locally shadowed areas; local homogeneity is almost an inverse function of inertia; energy maximizes for plain textures (i.e., no change in gray level); and entropy is similar to energy, but with a more prominent separation from plain texture.

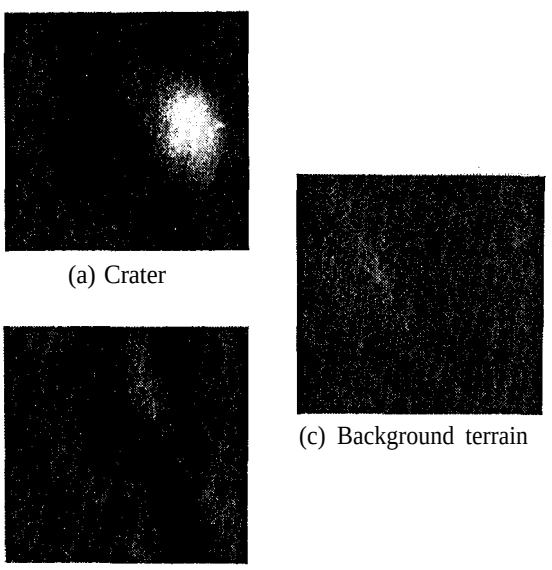

(a) Crater

(b) Valley

(c) Background terrain

Fig. 2. Regions selected for evaluation from the Fig. 1 Miranda image. These features are quite common in solar system bodies.

3. EXPERIMENTS

In the first set of experiments, we select three regions from the Miranda image of Fig, 1 for evaluating the performance of candidate feature detection metrics (see Fig. 2). The regions are 51x51 pixels in size. The detection matrics for different values of spacing parameter d given 0° θ-angle direction (i.e., no rotation) are computed using 8 gray levels. As shown in Fig. 3, inertia performs well for large d because the intensity is more likely to be randomly different; cluster shade and cluster prominence favor local binary light-dark regions, and thus prefer smaller d (note the sign change for crater and valley features in the cluster shade metric which is cubic is nature); local homogeneity is somewhat similar to inertia but with a high value. for small d that decreases as d increases, and separations of features from background are more prominent as d inc1 eases; energy and entropy, although their separations of feature from background are not extremely large in magnitude, possess a desirable property–constancy over a wide range of d–which simplifies the detection threshold determination. Cluster prominence is also a good candidate mainly because of the magnitude of feature and background separation for small d which simplifies the metric calculation.

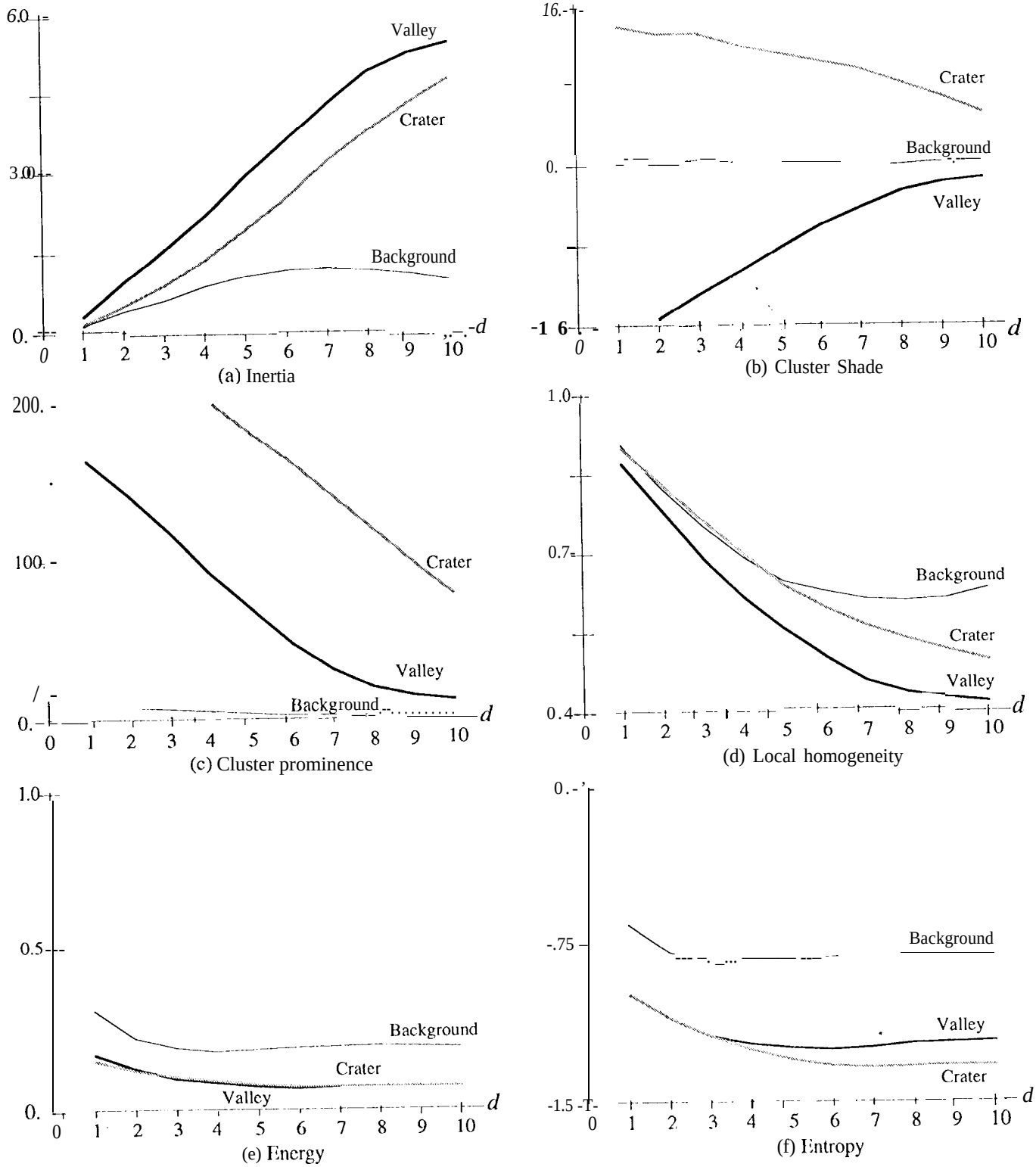

Fig. 3. Detection sensitivity y of candidate GLC-based metrics 1or the crater, valley, and background regions shown in Fig. 2. Cluster prominence performs extremely well for small cl, but entropy provides constancy in terms of feature/background separation over a wide range of d.

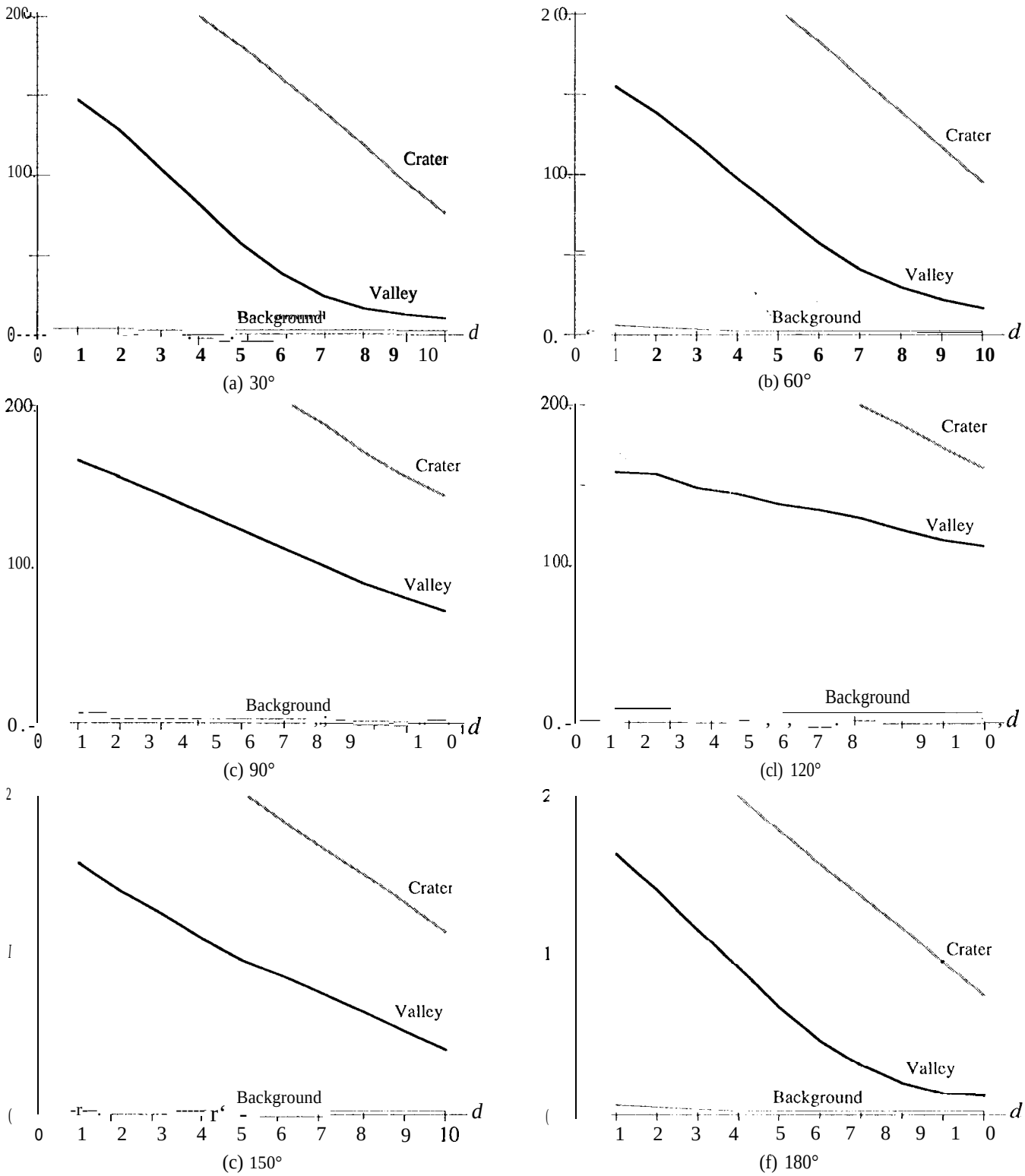

Fig. 4. Detection sensitivity of cluster prominence with respect to rotation for the crater, valley, and background regions shown in Fig. 2. Due to sufficient separation of features from background, feature detection may be achieved by applying an appropriate threshold to the measured cluster prominence value.

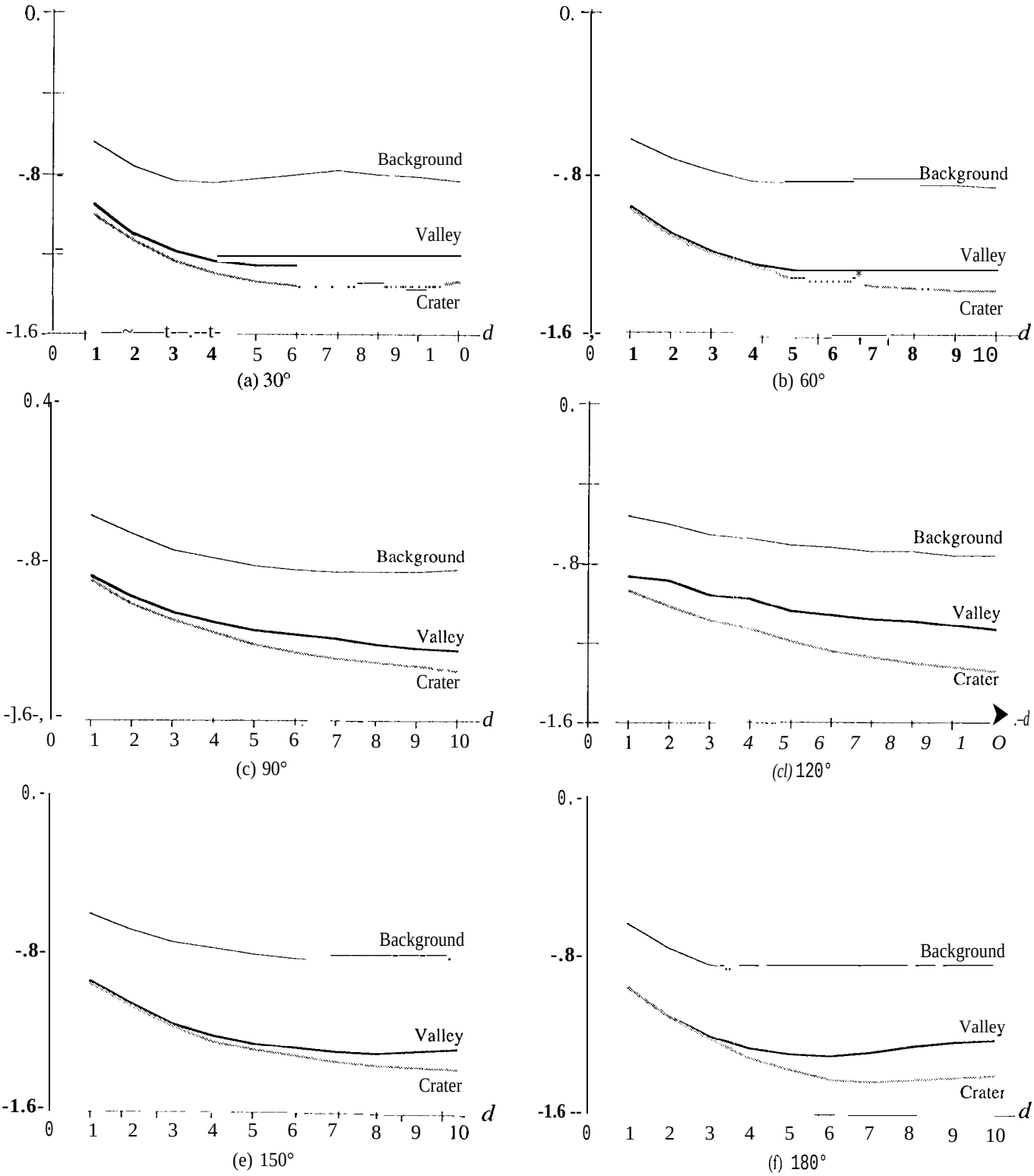

Fig. 5. Detection sensitivity of entropy with respect to rotation for the crater, valley, and background regions shown in Fig. 2. Of all the metrics, entropy is the least sensitive to feature orientation.

Rotation sensitivities with repect to the directional angle θ are also evaluated for all the metrics at every 30° interval. Results show that the crater region is not very sensitive to rotation. However, except for the energy and entropy metrics, separations from background for the valley region are significant] y distorted at 120° (this angle aligns one of the axes with the long-narrow stretch of the valley). Inertia and local homogeneity performance at 120° is worse than at other θ angles, while other metrics seem to improve the feature-background separation at this angle. Although the characteristics of cluster prominence significantly change at 120°, this does not jeopardize the ability to differentiate features from the nearby background terrain. Figures 4 and 5 demonstrate the detection sensitivity of cluster prominence and entropy with respect to θ (i.e., rotation).

In our next experiment, we wish to address the performance of candidate detection metrics for various types of planetary scenes and features. Figures 6-8 show the performance of cluster prominence and entropy on Triton, Io and Jupiter. Since the selected Io dark area and Jupiter regions are about twice the size of other selected regions, the d-increment for these regions is 2 instead of 1. To make this metric selection process more stringent, the same metric scalings' and ranges must be applied to all the different features and planetoids selected in this experiment. This would simplify the standardization of "distinct" feature definitions based on some a priori metric criteria.

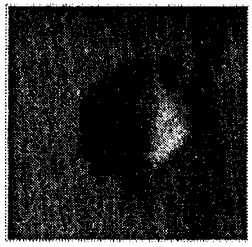

(a) Crater

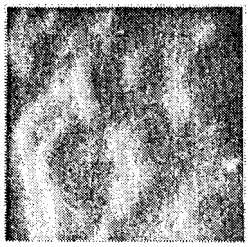

(c) Background

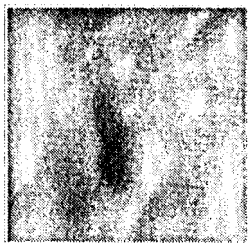

(b) Triple crater

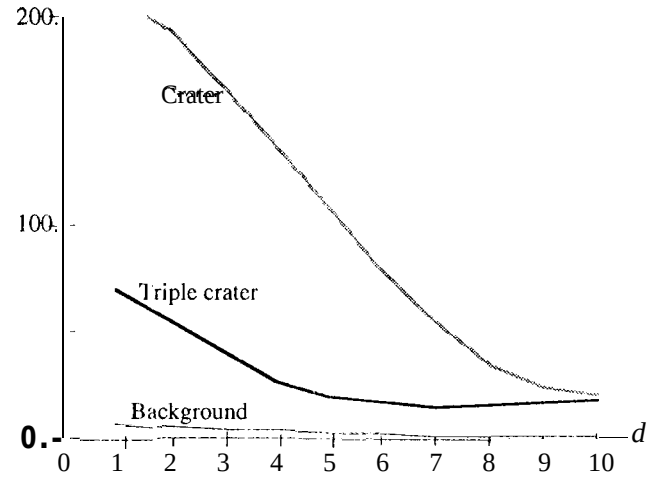

(d) Cluster prominence for 0° rotation

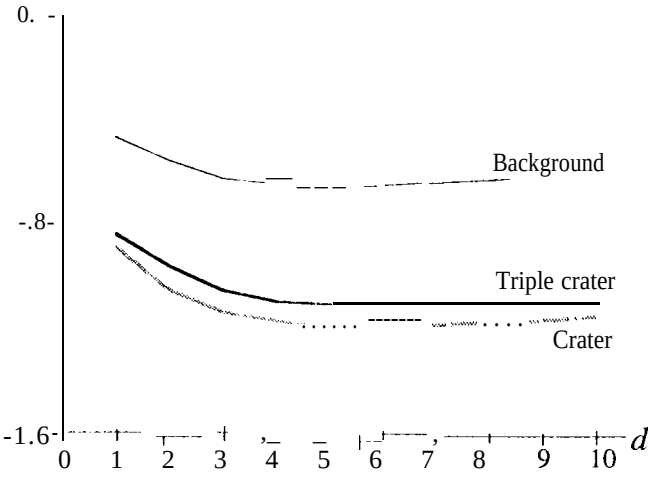

(e) Entropy for 0° rotation

Fig. 6. Regions selected for evaluation from the Fig. 1 Triton image. Cluster prominence performance degraded a little bit in comparison to the Miranda features. However, the entropy performance is holding steady in spite of differences in planetary scenes.

As shown in Fig. 6, cluster prominence performance on Triton again exhibits superior detectability at small d, as previously shown in the Miranda images (although the performance at high d is not as good). However, entropy (which has outperformed cluster prominence with respect to rotation sensitivity) appears to possess another desirable trait of being, to some extent, scene (topological/geological) invariant.

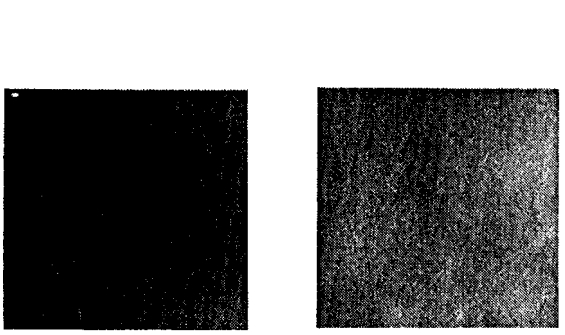

(a) Volcano

(c) Background

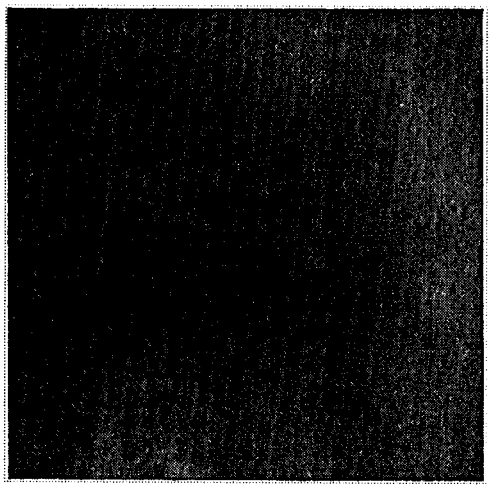

(b) Dark area

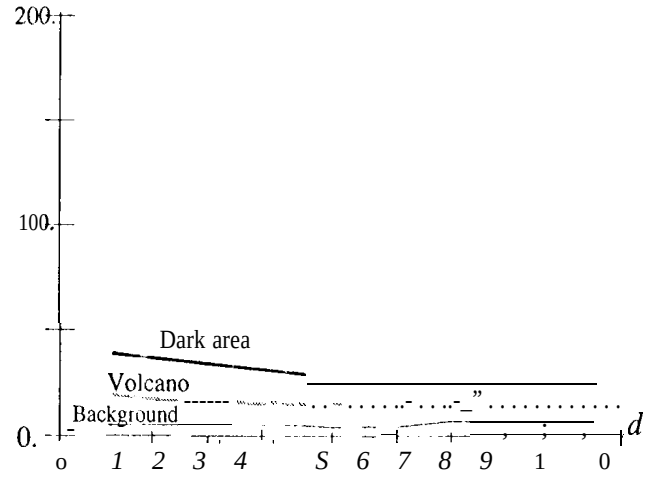

(d) Cluster prominence for 0° rotation

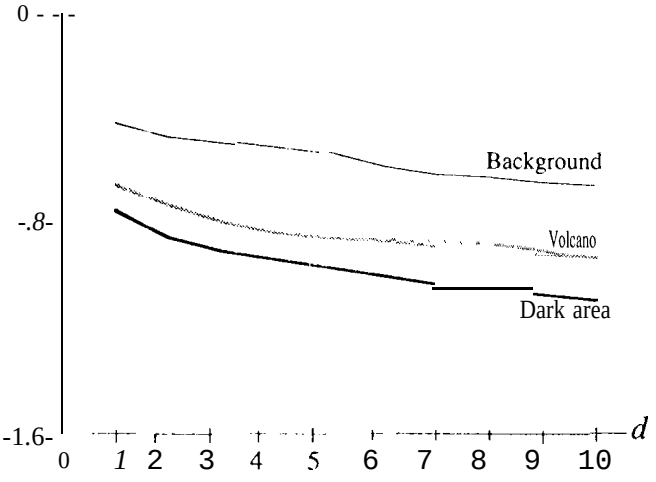

(e) Entropy for 0° rotation

Fig. 7. Regions selected for evaluation from the Fig. 1 Io image. Applying the same metric scalings and ranges for all the test images, detectability of cluster prominence significantly degraded, while entropy suffered only minor degradation,

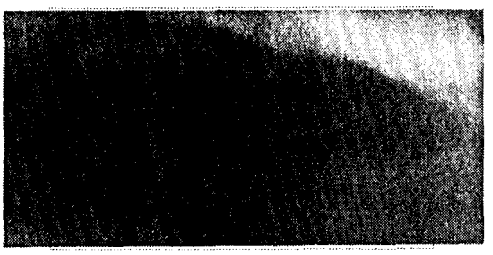

(a) Red spot

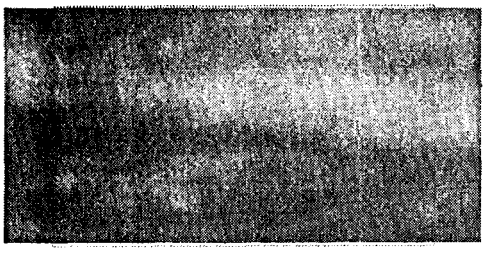

(c) Background

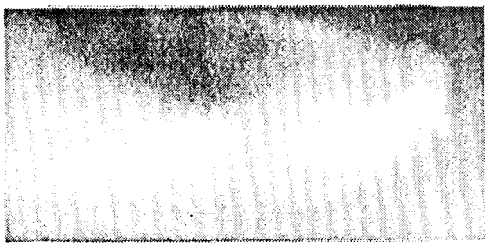

(b) Wave

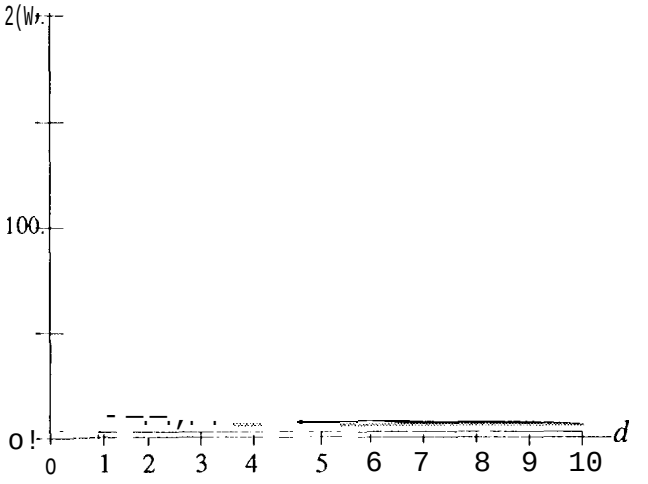

(d) Cluster prominence for 0° rotation

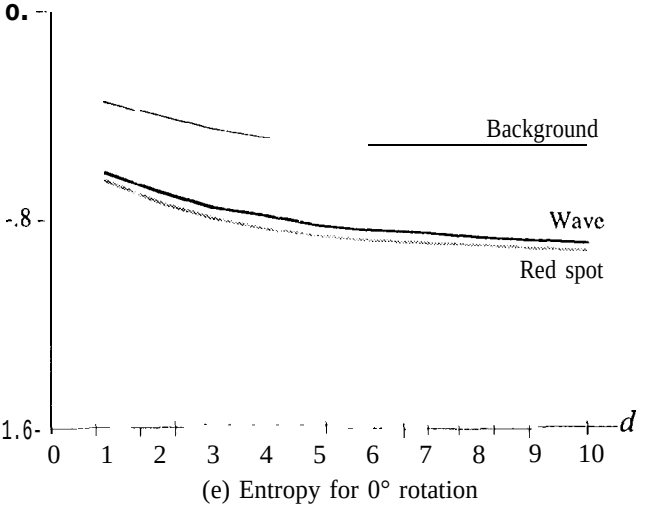

(e) Entropy for 0° rotation

Fig. 8. Regions selected for evaluation from the Fig. 1 Jupiter image. Complexity of the selected background regions renders cluster prominence ineffective. However, detectability performance of the entropy metric remains unchanged from scene to scene.

Figures 7-8 show the performance results of cluster prominence and entropy on different types of planetary features and background terrains. Io and Jupiter are very colorful, and their dynamic features (volcanoes and storms) are quite different from the static features (craters and valleys) of Miranda and Triton. As expected, the cluster prominence performance suffers from the different colors of natural background terrains. On the other hand, entropy appears to provide consistent detection performance for isolating "distinct" planetary features.

4. SUMMARY AND CONCLUSIONS

The primary goal of this study is to find an efficient way of autonomously detecting planetary features that is applicable to future exploration of known and unknown celestial bodies. In our opinion, classification of planetary features, such as craters, volcanoes, mountains, valleys, riverbeds, weather storms, geysers, etc., is better left to visual inspections by planetary scientists instead of trying to automate on board this very difficult perception process. Ground automation to locate patterns of

interest[8-9] does not have to deal with onboard computing limitations and lack of a priori knowledge. Furthermore, shading ambiguity with respect to the convexity of planetary surfaces can lead to misinterpretation of terrain features. 10 Thus, the focus remains on automating the detection of "distinct" planetary features that incorporates all the different features of scientific interest to permit effective data collection during planetary exploration. Looking at the different planetary images and arbitrarily selected interesting regions for this study, we believe that texture-based coupled with sharp-edge detection is typically desired (although this is not a scientific approach to test human perception ability). Preliminary results based on applying various GLC-based metrics accentuate the superiority of the entropy metric over others (with respect to sensitivities to rotation and terrain/geological differences) when dealing with planetary terrain features. More research to address prioritization of detected features is needed, and work to formulate, test and improve this feature detection process for autonomous planetary spacecraft is ongoing.

5 . ACKNOWLEDGMENTS

The authors would like to thank David Zhu for his programming assistance. The research described in this paper was carried out by the Jet Propulsion Laboratory, California Institute of Technology, under a contract with the National Aeronautics and Space Administration.

6 . REFERENCES

1. S. Udomkesmalee, G. E. Sevaston, and R. H. Stanton, "Toward an autonomous feature-based pointing system for planetary missions," *Proc. SPIE*, Vol. 1949, pp. 2-14, 1993.
2. C.-C. **Chu,** D. Q. Zhu, S. Udomkesmalee, and M. I. Pomcrantz, "Realization of autonomous image-based spacecraft pointing systems: Planetary flyby example," *Proc. SPIE*, Vol. 2221, pp. 27-40, 1994.
3. C. C. Liebe, "A new strategy for tracking planetary terrains," *Proc. SPIE*, Vol. 2221, pp. 41-55, 1994.
4. M. M. Trivedi and C. Chen, "Object detection by step-wise analysis of spectral, spatial, and topographic features," *Comput. Graphics Image Process.*, Vol. 51, pp. 235-255, 1990.
5. R. W. Conners and C. A. Harlow, "Toward a structural textural analyzer based on statistical methods," *Comput. Graphics Image Process.*, Vol. 12, pp. 224-256, 1980.
6. J. Weszka, C. Dyer, and A. Rosenfeld, "A comparative study of texture measures for terrain classification," *IEEE Trans. Sys. Man and Cybernet.*, Vol. SMC-6, pp. 269-285, April 1976.
7. M. M. Trivedi, C. A. Harlow, R. W. Conners, and S. Gob, "Object detection based on gray level cooccurrence," *Comput. Graphics Image Process.*, Vol. 28, pp. 199-219, 1984.
8. M. C. Burl, U. M. Fayyad, P. Perona, and P. Smyth, "Automated analysis of radar imagery of Venus: handling lack of ground truth," *Proceedings of the 1994 IEEE Conference on Image Processing*, Austin, Texas, November 1994.
9. M. C. Burl, U. M. Fayyad, P. Perona, P. Smyth, and M. P. Burl, "Automating the hunt for volcanoes on Venus, " *Proceedings of the 1994 IEEE Computer Vision and Pattern Recognition Conference*, Seattle, Washington, June 1994.
10. A. P. Pentland, "Local shading analysis," *IEEE Trans. Pattern Anal. Much. Intelligence*, Vol. PAMI-6, pp. 170-187, March 1984.